Proceedings of the ASME 2020 15th International Manufacturing Science and Engineering Conference
MSEC2020
June 22-26, 2020, Cincinnati, OH, USA

MSEC2020-8345

TRANSIENT MELT POOL FORMATION IN LASER-POWDER BED FUSION PROCESS

Santosh Rauniyar[1], Kevin Chou
Department of Industrial Engineering
University of Louisville

ABSTRACT

Parts are built in a layer-by-layer fashion in the laser powder bed fusion process. Each layer of scan in the parts is defined by a scan strategy that consists of many small patches and scans. The scan length of those multiple scans is not always long enough to have reached a quasi-steady state of the melt pool. The length at which it achieves a steady state is different for different process parameters. The available literature related to the melt pool considers the melt pool has already achieved a steady state, which holds true to a large extent. However, there is always a transient state of melt pool with different characteristics compared to the quasi-steady state. The transient state of the melt pool is particularly significant for small features and thin walls. This paper explores the cross-section and width of the melt track in the transient state. Single-tracks are deposited on semi-cylindrical samples with Ti-6Al-4V powder particles for three levels of power and speed combinations. The single tracks are built at a certain height from the base plate instead of on the build plate to include the effect of the powder particles. The experiment includes single tracks of four scan lengths i.e. 0.25, 0.5, 1 and 2 mm. Once the parts are built and removed from the build plate, White light interferometer is used to capture the melt track information and data processing is done in Matlab ™. The results show that the transient length is directly proportional to the laser power and inversely proportional to the scan speed. The highest transient length value is obtained for the highest power of 195 W and lowest scan speed of 50 mm/s.

Keywords: Melt pool, Transient state, LPBF, Ti-6Al-4V

1. INTRODUCTION

Laser-powder bed fusion (LPBF) process has the ability to produce highly dense metals parts with complex geometrical features [1]. The advancement in this technology has enabled the user to create lightweight high-strength [2] and bio-inspired design structures [3], thin walls [4], and heat exchangers with internal features [5] that cannot be fabricated by conventional manufacturing methods. Many of these designs have small features, which have dimensions in the range of 1-2 mm or less. The characteristics of these features are not similar to the bulk components [6].

Three-dimensional parts are produced using LBPF process in a layer-by-layer fashion. The laser heat source is used to selectively melt the fine metallic powders in the order of microns that are spread over a substrate. It involves rapid heating, melting and fluid flow and cooling during the process. There is a complex interaction between the laser and the metallic powder, which is highly affected by the change in process parameters [7] [8]. This interaction in each layer is governed by a scanning strategy [9]. The scan strategy typically consists of many short segments instead of long passes to avoid residual thermal stress. The melt pool during the short segment scans is not consistently at a steady state.

The melt pool for long passes will reach a quasi-steady state after the laser beam travels a certain distance given that the scanning direction is unchanged [10]. The melt pool geometry before the quasi-steady state i.e., the transient state is quite different. Furthermore, the laser beam goes through a phase of acceleration or deceleration at turn points at which the melt pool exhibits different properties [11]. Overall, there are four scenarios; (a) melt pool for small features (b) smaller scan lengths due to the scan strategy (c) melt pool at the start and end of long scans (d) melt pool at laser turn points in powder bed fusion process where we can observe a transient state of melt pool. Single tracks of small scan lengths built with skywriting ON is investigated in this paper.

[1] Contact author: santosh.rauniyar@louisville.edu

Previous studies have analyzed the melt pool geometry for different process parameters in order to control the melt pool size. Birnbaum et al [12] were able to achieve a desired melt pool size in LENS^{TM} process using a process map approach. They successfully created a model to change the power or the velocity establishing a dynamic feedback control of melt pool. Aggarangsi et al [13] further expand the process map approach to study the response of melt pool size to step change in power and velocity. Soylemez et al [14] presented a map of curves of constant melt pool cross-sectional area and length to depth ratio for electron beam additive manufacturing (EBAM) established by analytical and numerical method. Fox et al [15] studied the melt pool depth of Ti-6Al-4V single tracks for a wide range of power (1-5kW) and velocities (1-100 in /min) for the EBAM process. The power and velocities used in this study is high compared to the parameters generally used in the LBPF process.

Cheng and Chou [16] developed a thermal model to study the melt pool in Inconel 718 in LPBF process. The simulation study concluded that the development of a melt pool is affected by the process parameters whereby a larger beam power and slower speed will cause an increase in the melt pool evolution distance. Obidigbo [17] studied the melt pool dimension of Invar36 using numerical and experimental approaches. The thesis concluded that the transient length varies with the change in process parameter and speed has more effect on the initial state of the melt pool. Powder particles are not included in both of these studies.

Studies have shown that the dimensional accuracy, porosity as well as the microstructure for thin features are different compared to the bulk structures [6] [18]. The thin feature structures have different thermal history and can have significant effect of changes in scan parameters, powder size and distribution. This size effect in the metal LBPF is largely unexplored. The aim of this study to generate enough data and information to understand the variations in smaller scan lengths in order to build three dimensional struts and lattice-included structures with higher dimensional accuracy and reliable quality.

2. EXPERIMENTAL DETAILS

In this study melt pool geometry of single tracks with length, less than and equal to 2 mm are analyzed. The single tracks are built with Ti-6AL-4V powder particles in EOS M270 machine. The machine is equipped with a 200 Watt Continuous wave Ytterbium fiber laser. The laser beam dimeter is 100 microns. The build was completed with Skywriting ON option. The acceleration and deceleration of the laser will not occur during the scan of single tracks. Once the build is complete, the built parts are removed from the build plate. The melt pool information from the as-built part is captured using a White light interferometer (WLI) scan. The data acquired from the WLI scan of the melt pool is further processed using Matlab.

2.1 Sample design and fabrication

A semi-cylindrical design was chosen to save material and build the single-track deposits at a certain height instead of on the build plate. Figure 1 shows the basic design and dimension of the sample. The sample has raised wall on either side along the length with notches to mark the position of the tracks. Three levels of power, three levels of speed and four levels of scan length were chosen for the experiment. Table 1 list the laser power and scan speed combination used in the experiment. The four scan lengths are 0.25, 0.5, 1 and 2mm. In total, there were 36 single-track deposits.

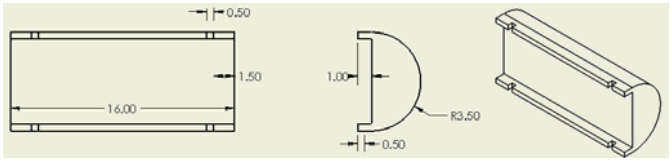

Figure 1. Semi- cylindrical sample with raised walls on either sides (Top, side and Isometric view).

Table 1. Scan parameters and linear energy density for the nine parameter combinations.

Speed (mm/s)	100	550	1000
Power (W)	Linear energy density (J/mm)		
50	0.500 (P1)	0.091 (P2)	0.050 (P3)
125	1.250 (P4)	0.227 (P5)	0.125 (P6)
195	1.950 (P7)	0.355 (P8)	0.195 (P9)

Thirty six tracks were arranged in two semi-cylindrical samples i.e., samples X and Y. The arrangement of tracks in sample Y is shown in Figure 2 below. Tracks with linear energy density (LED) less than 1 were created at a 1 mm gap and with LED greater than 1 at a 2 mm gap. The tracks with LED greater than 1 were kept in Sample Y. A number and letter code was used to identify the parameters and track length respectively. For example in P1A, P1 represents the parameter combination 1 i.e., power 50 W and a scan speed of 100 mm/s and A represents the scan length of 0.25 mm. Parameter combination coding is also presented in Table 1. For scan length, the letters A, B, C, and D indicate 0.25, 0.5, 1 and 2 mm lengths respectively. Nine replicates were built for both samples X and Y in two separate builds. EOS M 270 machine was used to build the samples. Apart from the single-track deposits, the samples were built at default parameters. Images of the samples on the build plate and zoomed view of one of sample Y is shown in Figure. 3.


Figure 2. Top view of the single tracks of length 0.25,0.5,1 and 2 mm arranged in sample Y.

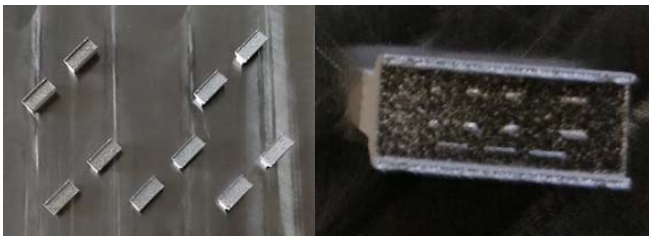

Figure 3. Five sets of Samples X and Y on the build plate (left), Zoomed view of the sample Y showing the single tracks(right).

2.2 Single-tracks surface morphology

A white light interferometer, NT1100 from Veeco Metrology, was used to collect the data of the single-track melt pool. The instrument was calibrated using a 10 µm step-height standard. Vertical scanning interferometry (VSI) measurement mode was chosen with an objective lens of 50X and a 0.5X field of view lens. This gives an effective field of view of 0.25 mm * 0.19 mm. Therefore, multiple scans had to be done to capture the entire melt pool of scan lengths 0.25, 0.5,1 and 2 mm in a single image. Multiple scans with a backscan of 250 µm and rectangular stitching function were used to acquire the images. The pixel resolution of the acquired image is approx. 339.5 nm * 396 nm. Figure 4 shows the sample setup for measurements. The semi-cylindrical sample is placed on the clay to avoid any sample movement in the duration of the WLI scan.

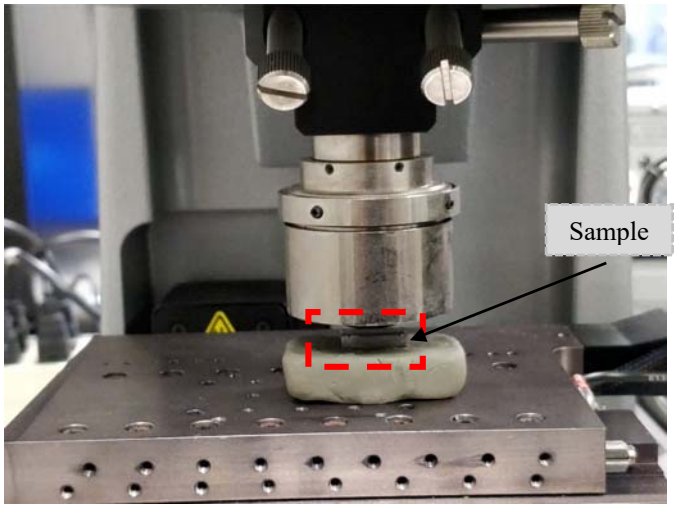

Figure 4. Sample setup for the measurement.

2.3 Data processing and width measurement

A typical image result from the WLI scan is shown in Figure 5. The black dots in the image are the pixels for which the scan did not acquire data. The software for the WLI scan has an option to restore the data for the bad pixels. A typical restored image result is shown in Figure 6. This option should not be used to restore large areas of bad data. Figure 7 shows the three-dimensional representation of the surface height.

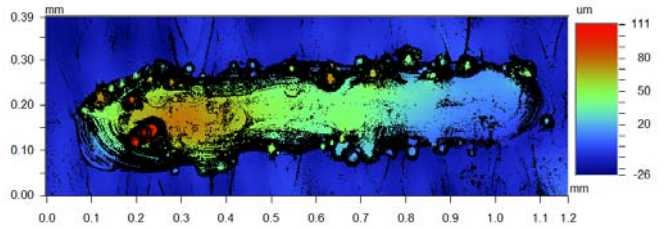

Figure 5. Acquired image from WLI scan for a typical case.

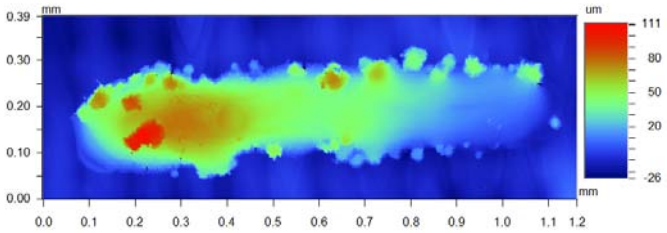

Figure 6. Data restored image.

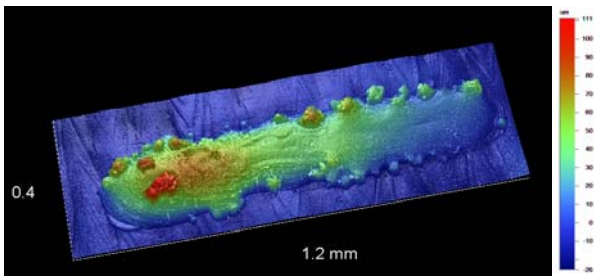

Figure 7. 3-Dimensional display of the melt pool.

MATLAB™ was used to calculate the width of the melt pool. The restored data matrix from the WLI was imported into the software. Each data in the matrix represents the surface height for a pixel of length 339.5 nm and width 396 nm. An algorithm using a first-order Savitzky-Golay filter with a frame length of twenty-one along with a cutoff value was used to obtain the melt pool width. The cutoff value was established by reviewing the surface height data of the first and last five columns and rows from the matrix. In an ideal case, the minimum value from those twenty surface height data was chosen as the cutoff value. The data obtained after applying the cutoff value is stored as a separate matrix data and considered as the melt pool. Due to the high density of the data, the color representation cannot be seen in Figure 8. For visualization purposes, this case is saved at a one-eighth resolution and the resulting image is shown in Figure 9. The data matrix for the reduced resolution has 214 columns and 63 rows. Figure 10 represents the melt pool with one-fourth resolution after filtering. The numbers on the X- and Y- axis in the figure represents the column and row number respectively instead of the track dimension. Melt pool width is calculated from the melt pool matrix data by subtracting the lower row number which indicates the lower end of the melt pool from higher row number which indicates the upper end of the melt pool in each column. This gives a width value for each data column from the melt pool data matrix.

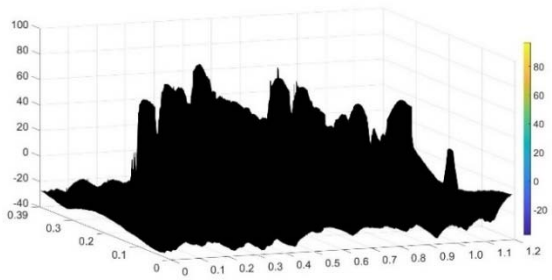

Figure 8. Surface height plotted from the entire data.

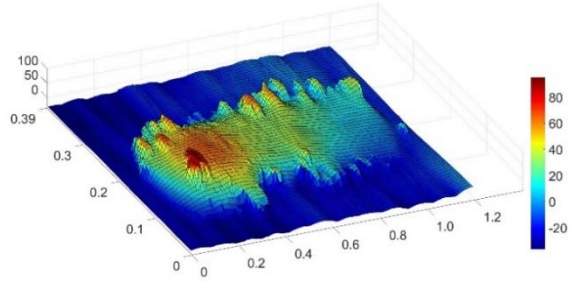

Figure 9. Surface height plot with one-eight data resolution.

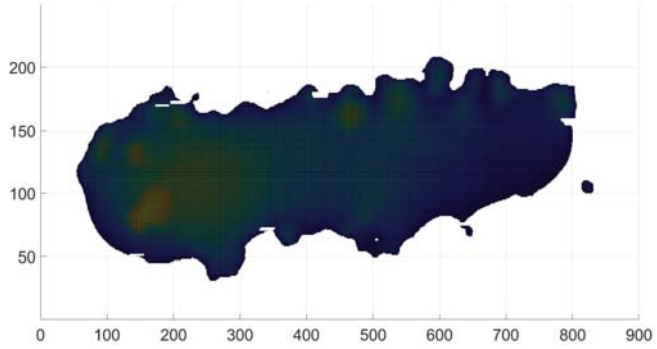

Figure 10. Top view of the melt pool after data filtering.

Width value was also calculated using edge detection on the original resolution tiff images files that are exported to Matlab after WLI scans. Canny method of edge detection technique was chosen after reviewing seven edge detection filters available in the Matlab. Figure 11 shows the result of using edge detection method on the full resolution image result of P8C from Replicate 1. This method can detect the edges of the track but with some exceptions. When the graph of the width along the scan length is plotted, we can clearly notice there are several missing data columns. This method was implemented in several other cases and the results were compared with the results from the cutoff value method. Overall, the trend of the melt pool width from both method is similar. But there is difference in the absolute width value in between the two methods. A graphical comparison of the width value for the P8C case is shown in Figure 13. There are certain data points with zero width value, near 800 mm scan length, which indicates that the edge detection method could not detect the track edge in all of the data columns. Therefore, cutoff method on processed data was used to calculate the width values instead of the edge detection on images.

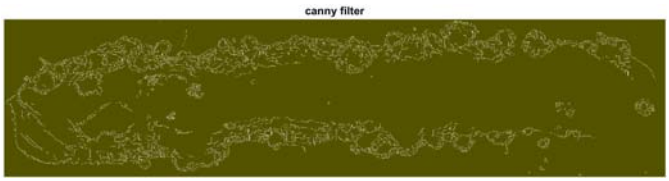

Figure 11. Image display after using canny edge detection.

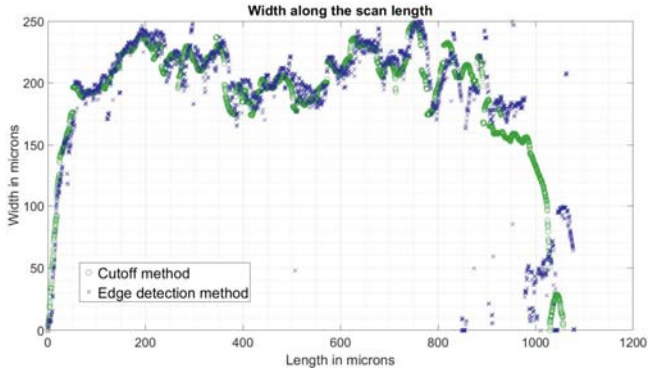

Figure 12. Comparison between the width value from cutoff method and edge detection method.

3. RESULTS AND DISCUSSION

3.1 WLI scan images

WLI scan images for 2mm scan length for nine parameter combination from one replicate is presented in Figure 13. The scan direction is from left to right. Parameter combinations P2 and P3 did not produce a continuous single track and was not considered for the melt pool geometry analysis. Melt pool at the start of the track, for the rest of the seven cases, shows higher surface height with semi-rounded shape while the end of the melt pool is flat and has low surface height. There are powder inclusions attached to the edges of the tracks on either sides as well as on other regions.

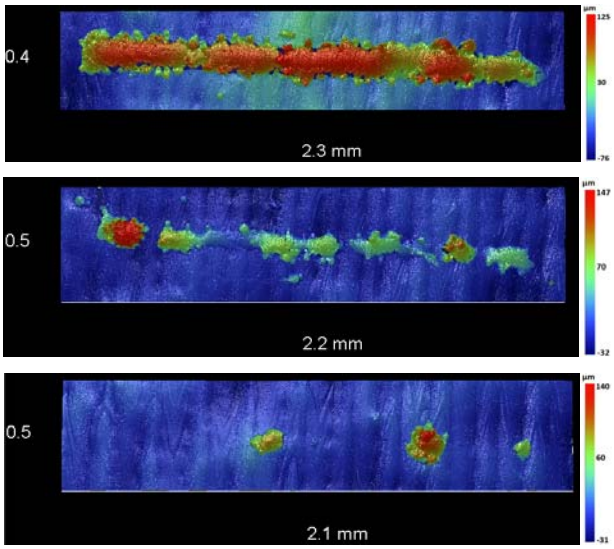

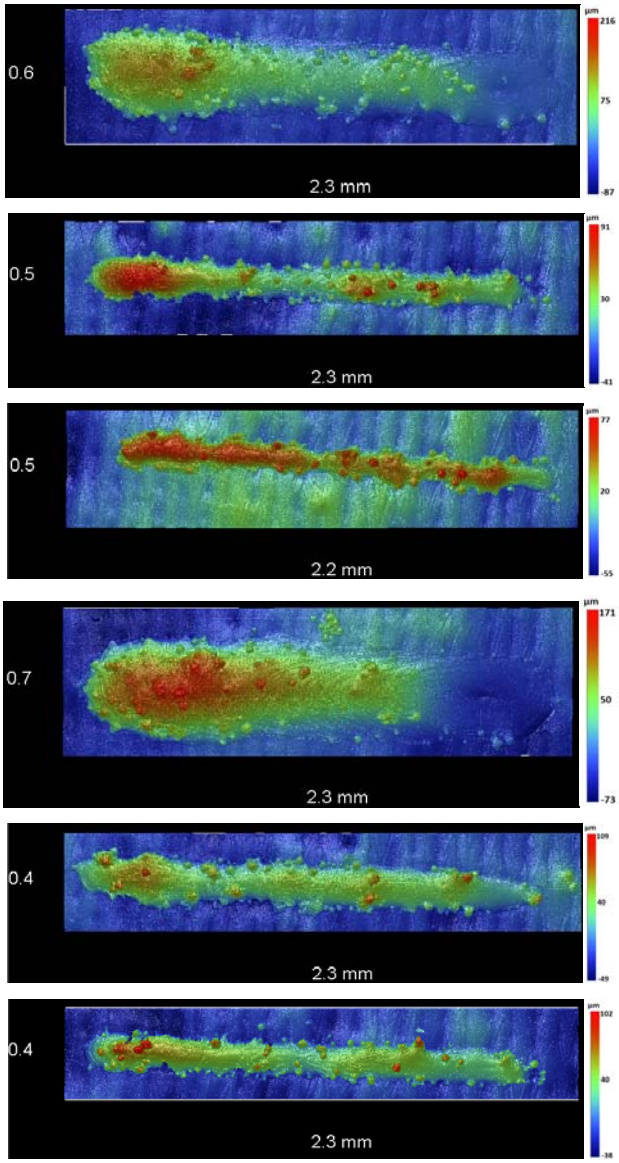

Figure 13. Entire set of nine parameter combination (P1 to P9 from top to bottom in order) results for 2 mm scan length from Replicate 1.

3.2 Melt pool width and cross-section

Melt pool width was calculated after filtering out the single track data from the data matrix imported from WLI. A single cutoff value was used to separate the melt pool data. After filtering, the data points with surface height less than cutoff value were removed and only the single track is stored in a separate data matrix. It is understood that using one single cutoff value can introduce error in some data columns because of the variable surface height all around the track. Each column has a surface height data for a pixel of length 339.5 nm. And only the initial portion of the melt pool is considered to find out the transient length. Taking these factors in consideration and after reviewing the melt pool curve at different cross-section, it was established that the error will be minimum at the start of the track. Therefore, a single cutoff value was considered suitable to separate the melt track for the purpose of finding the transient length at this stage of the study. Figure 14 shows the melt pool cross-section of 100 columns of data (from 0.187725 mm to 0.221671 mm, 0.033946 mm length) at the start of the track before and after filtering for the case P8C discussed in section 2.3. The melt pool width for these data columns is around 220µm.

F

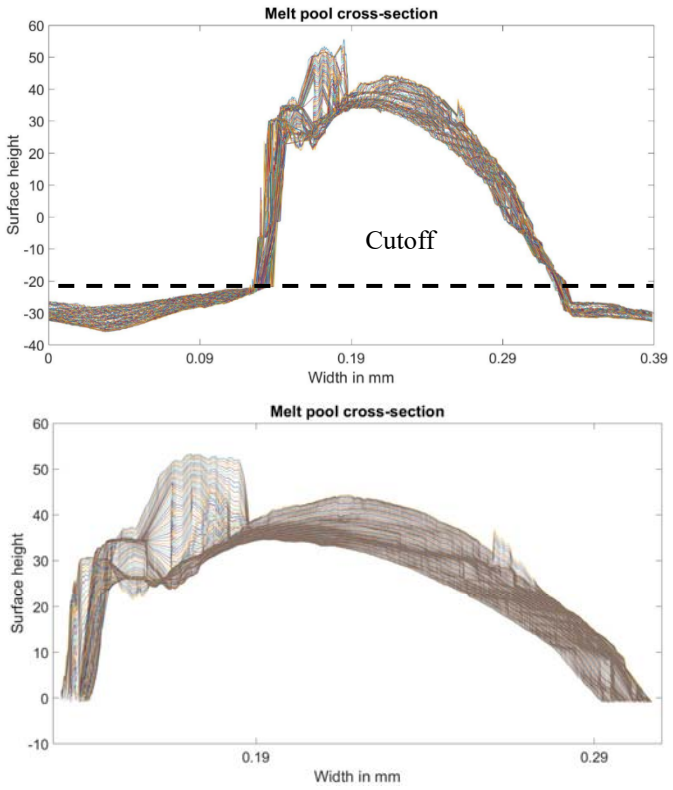

Figure 14. Melt pool cross-section from 100 data columns before and after filtering.

From the images in Figure 13, it is clear that the surface height for different parameter combinations is quite different. Therefore, a simple comparison of the surface height between parameter combination with lowest energy density P6 and highest energy density P7 is performed. Parameter combinations P2 and P3 are excluded while considering the lowest energy density because they did not produce a complete and consistent single track. Cross-section from a single data column in the middle region of the track is plotted in the graph presented in Figure 15. The graph shows that the single tracks from parameter P7 has a wider melt pool (~ 0.43 mm) compared to parameter P6 (~ 0.11 mm) for the same scan length .

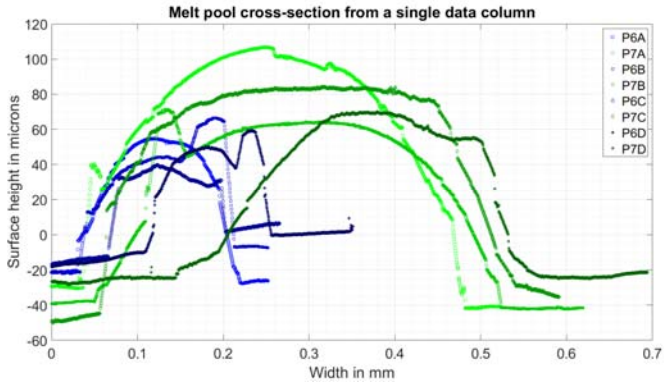

Figure 15. Graph showing the surface height variation as well as melt pool width variation between parameter combinations P6 and P7.

The melt pool shape at the start and end region of the single tracks shows different characteristics compared to the steady-state region. The melt pool cross-section across the width at four different regions for the case P7D is plotted. The melt pool cross-section from five adjacent data columns near the start of the track (at 0.0577 mm), the middle region of the track (at 0.9572 and 1.1270 mm) and near the end of the track (at 1.9926 mm) is plotted in Figure 16. The melt pool width slowly starts to increase from the start zone and reaches a steady- state in the middle region showing a semi-round shape. The melt pool width increase from approximately 0.22 mm to 0.50 mm. The end zone of the track is flat and the surface height matches the surface around it. Figure 17 shows the WLI scan result from replicate 2 for four scan lengths for parameter combination P6 and P7.

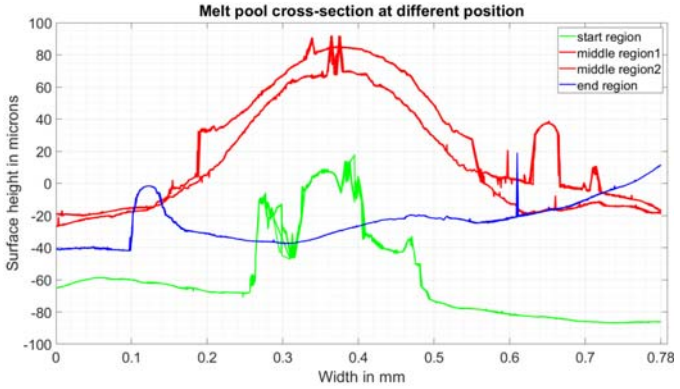

Figure 16. Melt pool cross-section at the start, the middle (2 points) and the end region.

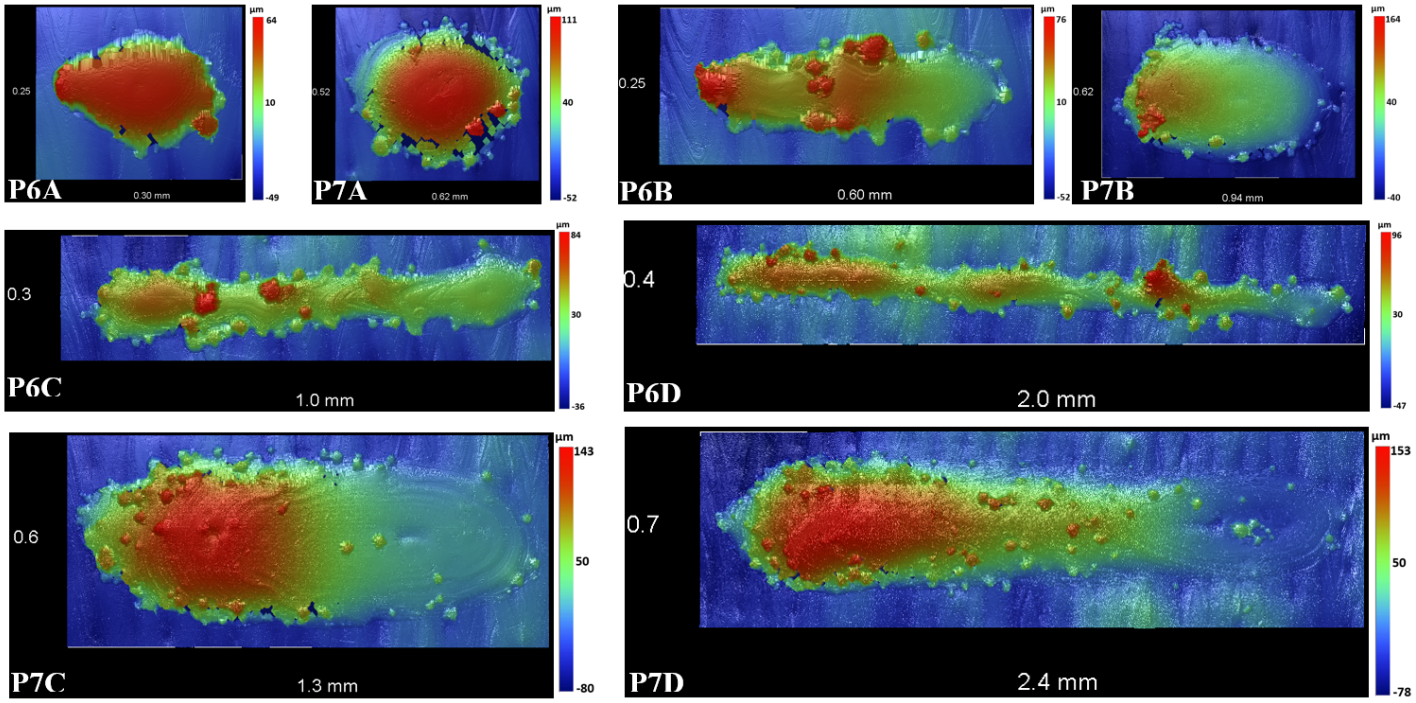

Figure 17. WLI scan images for four scan lengths for parameter combination P6 and P7 from replicate 2.

The melt pool width along the scan length is calculated based on the algorithm implemented in the Matlab. Width along the scan length was analyzed for all 28 cases, excluding 8 cases of parameters P2 and P3, of replicate 1. Melt pool width of tracks with four different scan lengths for parameter P6 is shown in Figure 18. The melt pool width for tracks with scan lengths of 0.25 and 0.5 mm does not reach a steady width value. The width peaks around 220 µm scan length for both cases. For scan lengths of 1 and 2 mm the melt pool width increases up to 410 and 450 µm respectively. This is the transient length (TL) after which the melt pool width becomes steady. The melt pool width shows slight fluctuation for tracks with scan length 1 mm and 2 mm even in the quasi-steady state. This variation in the melt pool width is due to the powder attached to the edges of the melt pool. Because of the attached powder particles, we do not observe a constant width value even after the transient length. For this study, the transient length is define as the position where a second peak width value is located in the scan length vs width graph. The second peak in the graph is the first peak point after the melt pool width decreases to its lowest value and then start to increase again. Figure 18 shows the calculated melt pool width along the scan length for a 2 mm scan for 3 replicates. The transient length for the three cases is around 650 µm.

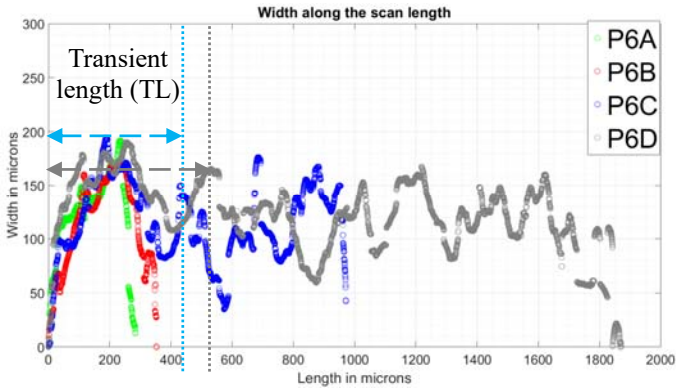

Figure 18. Calculated melt pool width of tracks for four different scan lengths of parameter case P6.

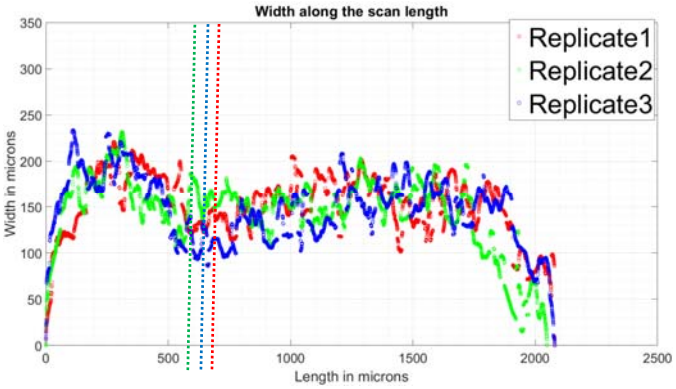

Figure 19. Calculated melt pool width for 2 mm scan length from 3 replicates for parameter case P5.

The melt pool width value of 28 single tracks of replicate 1 is calculated and analyzed. This includes the scan length of 0.25, 0.5, 1 and 2 mm. Afre reviewing the files, the transient lentgh for some parameter case was found to be higher than 1 mm. Therefore, the results from a 2 mm scan length were used to find the transient length for different parameter combinations from nine replicates.

3.3 Transient length

The melt pool geometry of the single tracks shows variation in both the surface height and the melt pool width for different process parameters. In addition, the melt pool width of a single track shows variation along the scan length. The variation is more apparent at the start and the end of the single tracks. This is because the melt pool is not at a quasi-steady state in that region. Transient length is the scan length from the start of the melt pool at which the melt pool has achieved a quasi-steady state. In this study, we can observe variation in the melt pool width even after the transient length. This is the attribute of the powder attached to the melt pool. Only melt pool width is considered as the parameter to differentiate between the transient and the quasi-steady state at this stage of the study. The scan length representing the second peak width value in the melt pool width vs scan length graph is established as the transient length. The melt pool width increases from zero to a certain peak value. After this, the melt pool width decreases up to some scan length. It reaches to the lowest width value. Then, there is an increase in the width again. The scan length at this point (peak width value) is identified as the transient length. Although the width value shows some variation (increase and decrease) even after this point. Similar trend is seen for all replicates as shown presented in Figure 18 above. The transient length for seven parameter combinations is calculated for nine replicates and the average values with their standard deviation is plotted as shown in Figure 20.

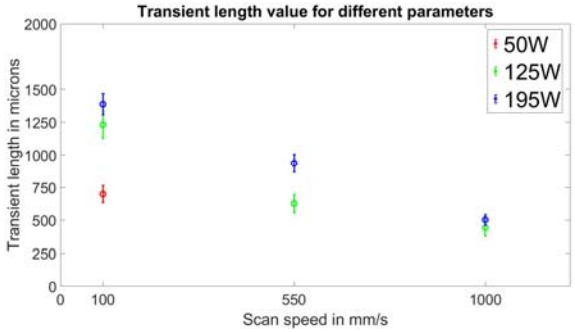

Figure 20. Caclulated transient length value for seven parameter combinations from nine replicates

The transient length for parameter case P7 is the highest with 1387 microns and P6 is the lowest with 443 microns. The transient length increase with the increase in power for all three scan speed. Whereas, the transient length decreases with an increase in speed for all three power cases. Because of the high standard deviation (60 – 100 microns), the transient length values for different parameters show some overlap.

4. CONCLUSION

This study is a first step towards understanding the characteristics of transient melt pool in the LPBF process. Single tracks of four scan lengths i.e., 0.25, 0.5,1 and 2 mm are built with Ti-6Al-4V powder particles. A combination of three levels of power and three levels of scan speed are used to deposit the single tracks on semi-cylindrical samples at a height of 6.63 mm from the base plate. WLI scan is done on the as-built samples to acquire the melt pool geometry information. Melt pool cross-section for different parameters at different positions of the single track is analyzed. An algorithm is implemented in Matlab to separate the melt pool of the single tracks from the surface. Melt pool width value along the scan length is also generated from the separated data. The transient length for seven parameter combinations is calculated from the melt pool width data. The results obtained can be summarized as

1) Melt pool geometry at the start and the end of the single track is different compared to the quasi-steady state.
2) Melt pool at the start of a single track is a semi-rounded shape with higher surface height. The end of the melt pool is almost flat and the surface height is very low similar to the surface around it.
3) Laser power and scan speed significantly affect the melt pool dimension as well as the transient length.
4) For a constant speed, the increase in power causes an increase in transient length given that other parameters remain unchanged.
5) For a given power, the increase in speed results in a decrease in transient length given that other parameters remain unchanged.

The powder attached to the melt pool adds complexity in separating the single track from the surface. More precise way of separating the melt pool will be explored in the future. At this stage, only the melt pool width was the parameter considered to determine the transient length. In the next step, a combination of melt pool width and surface height will be used to determine the transient length value. At the start of the study, there was no quantitative information on the transient length of the melt pool. Therefore, single tracks deposits of four small scan length were built. In the future, a wider range of combinations of power and scan speed will be used to deposit single tracks greater than and equal to 1 mm to determine the transient length. Simultaneously, modeling and simulation of the melt pool evolution will be carried out. In addition, the experiment will be carried out for different powder materials. Furthermore, the transient melt pool will be studied in two-dimensional raster-area scans and three-dimensional individual strut fabrications.

ACKNOWLEDGEMENTS

This research is supported by National Science Foundation award 1921263.

REFERENCES

[1] Schmidt, M., Merklein, M., Bourell, D., Dimitrov, D., Hausotte, T., Wegener, K., Overmeyer, L., Vollertsen, F., and Levy, G. N., 2017, "Laser Based Additive Manufacturing in Industry and Academia," CIRP Ann., 66(2), pp. 561–583.

[2] du Plessis, A., Yadroitsava, I., and Yadroitsev, I., 2018, "Ti6Al4V Lightweight Lattice Structures Manufactured by Laser Powder Bed Fusion for Load-Bearing Applications," Opt. Laser Technol., 108, pp. 521–528.

[3] Lin, K., Yuan, L., and Gu, D., 2019, "Influence of Laser Parameters and Complex Structural Features on the Bio-Inspired Complex Thin-Wall Structures Fabricated by Selective Laser Melting," J. Mater. Process. Technol., 267(November 2018), pp. 34–43.

[4] Calignano, F., Cattano, G., and Manfredi, D., 2018, "Manufacturing of Thin Wall Structures in AlSi10Mg Alloy by Laser Powder Bed Fusion through Process Parameters," J. Mater. Process. Technol., 255(February), pp. 773–783.

[5] Saltzman, D., Bichnevicius, M., Lynch, S., Simpson, T. W., Reutzel, E. W., Dickman, C., and Martukanitz, R., 2018, "Design and Evaluation of an Additively Manufactured Aircraft Heat Exchanger," Appl. Therm. Eng., 138(November 2017), pp. 254–263.

[6] Yang, L., Gong, H., Dilip, S., and Stucker, B., 2014, "An Investigation of Thin Feature Generation in Direct Metal Laser Sintering Systems," Proc. 26th Annu. Int. Solid Free. Fabr. Symp., pp. 714–731.

[7] Bidare, P., Bitharas, I., Ward, R. M., Attallah, M. M., and Moore, A. J., 2018, "Fluid and Particle Dynamics in Laser Powder Bed Fusion," Acta Mater., 142, pp. 107–120.

[8] Matthews, M. J., Guss, G., Khairallah, S. A., Rubenchik, A. M., Depond, P. J., and King, W. E., 2017, "Denudation of Metal Powder Layers in Laser Powder-Bed Fusion Processes," Addit. Manuf. Hand b. Prod. Dev. Def. Ind., 114, pp. 677–693.

[9] Anam, A., Dilip, J. J. S., Pal, D., and Stucker, B., 2014, "Effect of Scan Pattern on the Microstructural Evolution of Inconel 625 during Selective Laser Melting," Int. Solid Free. Fabr. Symp. – An Addit. Manuf. Conf., pp. 363–376.

[10] Scipioni Bertoli, U., Wolfer, A. J., Matthews, M. J., Delplanque, J. P. R., and Schoenung, J. M., 2017, "On the Limitations of Volumetric Energy Density as a Design Parameter for Selective Laser Melting," Mater. Des., 113, pp. 331–340.

[11] Martin, A. A., Calta, N. P., Khairallah, S. A., Wang, J., Depond, P. J., Fong, A. Y., Thampy, V., Guss, G. M., Kiss, A. M., Stone, K. H., Tassone, C. J., Nelson Weker, J., Toney, M. F., van Buuren, T., and Matthews, M. J., 2019, "Dynamics of Pore Formation during Laser Powder Bed Fusion Additive Manufacturing," Nat. Commun., 10(1), pp. 1–10.

[12] Birnbaum, A., Aggarangsi, P., and Beuth, J., 2003, "Process Scaling and Transient Melt Pool Size Control in Laser-Based Additive Manufacturing Processes," Proc. 14th Solid Free. Fabr. Symp., pp. 328–339.

[13] Aggarangsi, P., Beuth, J. L., and Gill, D. D., 2004, “Transient Changes in Melt Pool Size in Laser Additive Manufacturing Processes,” Proc. 15th Solid Free. Fabr. Symp., pp. 163–174.

[14] Soylemez, E., Beuth, J. L., and Taminger, K., 2010, “Controlling Melt Pool Dimensions over a Wide Range of Material Deposition Rates in Electron Beam Additive Manufacturing,” 21st Annu. Int. Solid Free. Fabr. Symp. - An Addit. Manuf. Conf. SFF 2010, (January 2010), pp. 571–582.

[15] Fox, J., and Beuth, J., 2013, “Process Mapping of Transient Melt Pool Response in Wire Feed E-Beam Additive Manufacturing of Ti-6Al-4V,” 24th Int. SFF Symp. - An Addit. Manuf. Conf. SFF 2013, pp. 675–683.

[16] Cheng, B., and Chou, K., 2015, “Melt pool evolution study in selective laser melting,” 26th Annu. Int. Solid Free. Fabr. Symp. - An Addit. Manuf. Conf. SFF 2015, August 10–12 (2015), pp. 1182-1194

[17] Obidigbo, C. N., 2017, “A Numerical and Experimental Investigation of Steady-State and Transient Melt Pool Dimensions in Additive Manufacturing of Invar 36.”

[18] Vilardell, A. M., Takezawa, A., du Plessis, A., Takata, N., Krakhmalev, P., Kobashi, M., Yadroitsava, I., and Yadroitsev, I., 2019, “Topology Optimization and Characterization of Ti6Al4V ELI Cellular Lattice Structures by Laser Powder Bed Fusion for Biomedical Applications,” Mater. Sci. Eng. A, 766(June), p. 138330.